Volume 10 | Number 6 | 16 March 2026

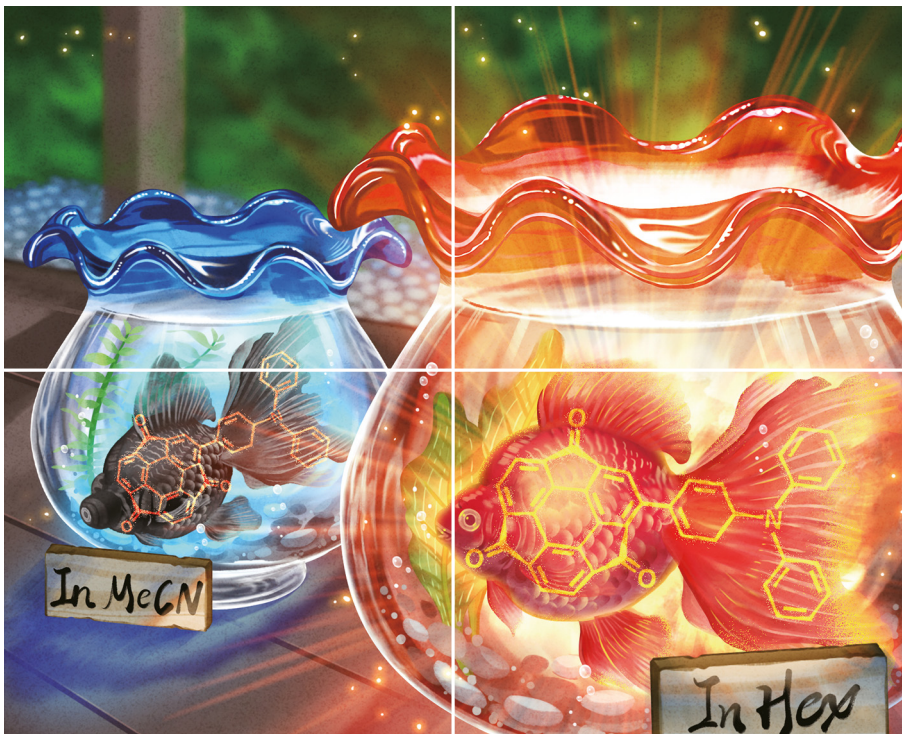

MATERIALS CHEMISTRY

FRONTIERS

CCS 中国化学会 CHINESE CHEMICAL SOCIETY
ICCAS 1956
ROYAL SOCIETY OF CHEMISTRY
rsc.li/frontiers-materials

MATERIALS CHEMISTRY FRONTIERS

CHINESE CHEMICAL SOCIETY

ROYAL SOCIETY OF CHEMISTRY

RESEARCH ARTICLE

View Article Online
View Journal | View Issue

Cite this: *Mater. Chem. Front.*, 2026, **10**, 938

High quantum yield NIR emission *via* charge transfer states in buckybowl-TPA based D–A systems

Yumi Yakiyama, *[abc] Junyi Han,[a] Hayato Sakai, *[d] Taku Hasobe,[d] Youhei Takeda,[a] Ryohei Kishi,[be] Kei Ohkubo[fg] and Hidehiro Sakurai *[ab]

The development of highly efficient near-infrared (NIR) emissive materials presents tremendous opportunities across diverse applications, from biological imaging to advanced optoelectronics. While planar aromatic dyes have traditionally dominated this field, we report herein the successful design and synthesis of a novel bowl-shaped NIR dye, **TPA-TOS**, incorporating the rarely emissive trioxosumanene (**TOS**) as the acceptor and triphenylamine (**TPA**) as the donor. In polar solvents, **TPA-TOS** exhibited weak luminescence confined to the UV region; however, in nonpolar environments, it demonstrated intense NIR emission spanning the 650 to 850 nm range. Remarkably, a quantum yield exceeding 60% in the NIR range was achieved, attributed to an intriguing photo-relaxation pathway. This mechanism involves exciton relaxation from localized excitation to the charge transfer (CT) state, mediated by thermally activated delayed fluorescence (TADF) between CT singlet and triplet states, along with room-temperature phosphorescence (RTP), ultimately transitioning to a long-lived charge-separated (CS) state. The outstanding amphiphilic nature, high quantum yield of NIR dual emission enabled by TADF and RTP, and the generation of a long-lived CS state are likely driven by the pronounced spin–orbit coupling facilitated by the curved sumanene skeleton. This work establishes **TPA-TOS** as a platform for NIR materials and insights into non-planar photophysics.

Received 18th November 2025,
Accepted 26th January 2026

DOI: 10.1039/d5qm00818b

rsc.li/frontiers-materials

Introduction

Near-infrared (NIR) dyes have garnered significant attention due to their vast array of applications in solar cells,[1] organic light-emitting diodes (OLEDs),[2] organic field-effect transistors (OFETs),[3] and various biochemical fields.[4] Beyond optoelectronics, NIR dyes have proven highly effective in tissue imaging and photopharmacology, owing to the minimal absorption and autofluorescence of biological tissues in the NIR range (700–1000 nm).[5,6] The design strategy for organic NIR dyes typically revolves around the donor–π–acceptor (D–π–A) paradigm, which facilitates intramolecular charge transfer (ICT) by modulating the frontier orbital energies—destabilizing the HOMO of the donor and stabilizing the LUMO of the acceptor—to precisely tune the energy gap between the ground and excited states.[7] Numerous factors influence the photophysical behavior of such systems, including the nature and arrangement of electron-rich and electron-deficient chromophores, the functionalization and conjugation style of linkers bridging donor and acceptor units, their spatial distance, and environmental conditions. The efficiency and dynamics of charge transfer are largely governed by electronic coupling and solvent polarity: stronger electronic coupling promotes orbital overlap and enhances CT character, while polar solvents stabilize the CT state *via* dielectric screening, increasing the population of CT species.

Over the years, various π-conjugated charge transfer molecules and polymers have been developed for NIR applications such as LEDs and *in vivo* imaging.[8] These materials often employ well-known strong electron acceptors, including benzothiadiazole (BT),[9] benzobisthiadiazole (BBT),[10] thiadiazoloquinoxaline (TQ),[11] triazolobenzothiadiazole (BTT),[12] diketopyrrolopyrrole

[a] *Division of Applied Chemistry, Graduate School of Engineering, The University of Osaka, 2-1 Yamadaoka, Suita, Osaka 565-0871, Japan. E-mail: yakiyama@chem.eng.osaka-u.ac.jp*
[b] *Innovative Catalysis Science Division, Institute for Open and Transdisciplinary Research Initiatives (ICS-OTRI), The University of Osaka, 2-1 Yamadaoka, Suita, Osaka 565-0871, Japan*
[c] *PRESTO, Japan Science and Technology Agency (JST), 4-1-8 Honcho, Kawaguchi, Saitama 332-0012, Japan*
[d] *Department of Chemistry, Faculty of Science and Technology, Keio University, Yokohama, Kanagawa 223-8522, Japan*
[e] *Department of Materials Engineering Science, Graduate School of Engineering Science, The University of Osaka, Toyonaka, Osaka 560-8531, Japan*
[f] *Institute for Open and Transdisciplinary Research Initiatives (OTRI), The University of Osaka, 1-6 Yamadaoka, Suita, Osaka 565-0871, Japan*
[g] *Organization for Carbon Neutrality Collaboration (OCNC), The University of Osaka, 1-6 Yamadaoka, Suita, Osaka 565-0871, Japan*

(DPP),[13] thienopyrroledione (TPD),[14] and boron-dipyrromethene (BODIPY).[15] However, such planar systems often suffer from strong π–π stacking, aggregation-induced quenching, and limited regulation of excited-state dynamics, which restrict their emission efficiency and multifunctionality. In contrast, non-planar conjugated molecules with twisted or distorted molecular geometries have recently emerged as an effective strategy to overcome these limitations.[16] Zhao *et al.* reported a hybrid planar–twisted indoline donor that balances π-conjugation and molecular distortion, enabling bright near-infrared emission in both molecular and aggregated states.[17] Sun *et al.* demonstrated that pyrazine-fused trichalcogenasumanenes with a non-planar π-conjugated framework enable effective excited-state regulation through triplet-state involvement, highlighting the role of molecular curvature in tuning excited-state dynamics.[18] These studies indicate the feasibility of employing non-planar molecular structures for near-infrared emissive materials.

Recently, trioxosumanene (**TOS**), a tri-oxidized bowl-shaped derivative of sumanene, has emerged as a promising multi-step electron acceptor due to its exceptional electron-withdrawing capability, with reduction potentials surpassing those of fullerene derivatives (Fig. 1).[19,20] Interestingly, **TOS** displays such pronounced electron-accepting properties that even strongly electron-deficient groups like nitrophenyl can function as donors when paired with it.[21] Additionally, as a typical π–π* triplet molecule, **TOS** exhibits rapid intersystem crossing (ISC) from the triplet state to the ground state (S_0), facilitated by a large spin–orbit coupling (|SOC|) due to its curved, non-planar structure.[22] These unique features make **TOS** highly attractive for applications in electron injection and the development of organic phosphorescent materials.

In this study, we present the design and synthesis of **TPA-TOS**, a **TOS**-based donor–acceptor NIR dye with a distinctive molecular architecture (Fig. 1). Featuring the bulky triphenylamine (**TPA**) group as the donor and **TOS** as the acceptor, the system achieves efficient intramolecular charge transfer (ICT), resulting in a narrowed bandgap and weak absorption extending into the NIR range up to 850 nm. Remarkably, **TPA-TOS** demonstrated an impressive quantum yield exceeding 60% in non-polar solvents such as hexane, with strong NIR emission spanning the 650–850 nm range. Femtosecond transient absorption spectroscopy (fsTA), electron spin resonance (ESR), and density functional theory (DFT) calculations suggest that the emission arises from thermally activated delayed fluorescence (TADF) and room-temperature phosphorescence (RTP), accompanied by partial charge separation. Furthermore, **TPA-TOS** exhibited distinct solvent dependency, showing negligible emission in polar solvents like acetonitrile (MeCN). With its unique mechanism and simplified donor–acceptor architecture, **TPA-TOS** paves the way for the development of efficient NIR dyes and highlights the tremendous potential of bowl-shaped molecular frameworks for advanced optoelectronic and biomedical applications.

Results and discussion

Synthesis and characterization of TPA-TOS

Fig. 2(a) illustrates the synthetic route to **TPA-TOS**. Bromotrioxosumanene (**TOS-Br**) was found to be a versatile precursor for obtaining various **TOS** derivatives[18] *via* an acidic Suzuki–Miyaura coupling reaction,[20] which avoids the basic conditions, under which the sumanene skeleton is relatively unstable. Resulting **TPA-TOS** was obtained as a dark-green solid and its structure was characterized by high-resolution mass spectrometry (HRMS) and ^{1}H and ^{13}C NMR spectroscopy (Synthetic details, NMR Spectrum S1–S3, SI). Although **TPA-TOS** had strong electron- accepting and electron-donating groups, resulting in a low HOMO–LUMO gap (1.809 eV at B3LYP/6-311+G(d,p)), it was stable under air and underwent only partial decomposition even at 400 °C. Interestingly, **TPA-TOS** was soluble not only in polar solvents such as MeCN and EtOH, but also in non-polar solvents such as hexane. This was probably attributed to the

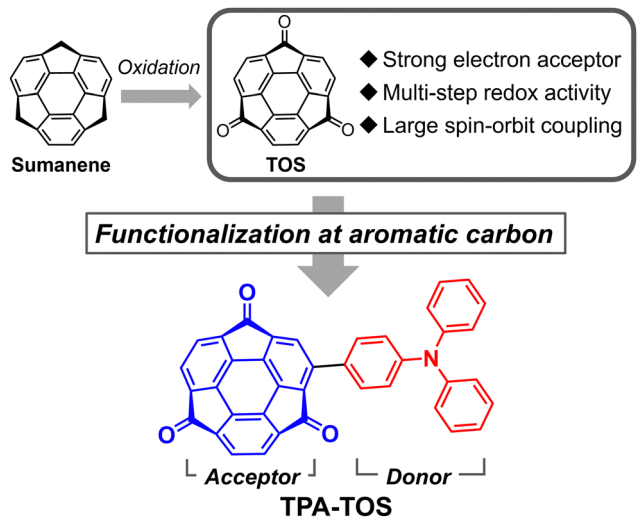

Fig. 1 Features of **TOS** and the schematic drawing of **TPA-TOS**.

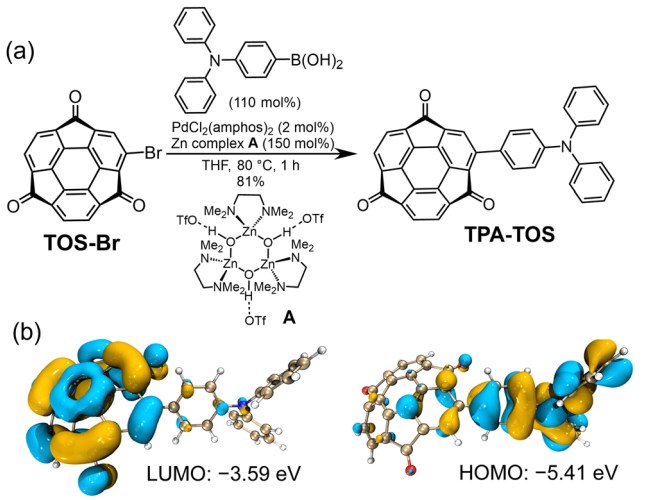

Fig. 2 Basic properties of **TPA-TOS**. (a) Synthetic procedure of **TPA-TOS**. (b) HOMO and LUMO distribution of **TAP-TOS** calculated at B3LYP/6-311+G(d,p) level.

curved structure of **TOS** moiety, in which partial dipole generates along the out of the plane direction of the bowl. Such carbon rich molecular skeleton with polarity realized the amphiphilic nature of **TPA-TOS**. Tremendous amounts of trials to get single crystals of **TPA-TOS** did not work to afford high quality crystal enough for single crystal X-ray diffraction analysis. Probably large **TPA** moiety disturbed the effective stacking formation of **TOS** moiety, giving only small low-quality crystals.

The electronic properties of **TPA-TOS** were next investigated. Density functional theory (DFT) calculations revealed that the HOMO was primarily localized on the **TPA** moiety, while the LUMO resided on the **TOS** skeleton, with slight orbital overlaps within each segment (Fig. 2(b)). Cyclic voltammetry (CV) and differential pulse voltammetry (DPV) measurements in MeCN containing 0.1 M of Bu_4NClO_4 as an electrolyte under a nitrogen atmosphere exhibited two distinct reversible reduction peaks at −0.79 V and −1.27 V at a scan rate of 10 mV s^{-1} (Fig. S1). This implied a strong electron-accepting ability of **TPA-TOS** reaching C_{60} as confirmed in **TOS** (−0.92 V and −1.43 V in THF).[19,23] Meanwhile, the observed oxidation peak of **TPA-TOS** at +0.55 V indicated the slightly lower donating ability of the **TPA** part on **TPA-TOS** than the unmodified **TPA** (+0.58 V in MeCN)[24] due to the conjugation with electron-accepting **TOS**. Both HOMO and LUMO energy levels were calculated from the onset potentials (E_{onset}) to be −3.72 and −5.25 eV, respectively.[25] These values were in good agreement with the DFT-calculated values.

Spectroscopic analyses

To gain insight into the fundamental optical properties of **TPA-TOS**, both absorption and fluorescence spectra were measured (Fig. 3(a) and Table 1 and Table S1). The acceptor unit, **TOS**, exhibited short-wavelength absorption in the UV region, characterized by an absorption coefficient (ε) of 1.0 × 10^4 M^{-1} cm^{-1} at 300 nm (Fig. S2). In contrast, **TPA-TOS** displayed distinct and intense absorption bands between 300–450 nm (ε = 7.6 × 10^4 M^{-1} cm^{-1} at 300 nm in acetonitrile), along with a prominent absorption band spanning 600–800 nm (ε = 1.2 × 10^4 M^{-1} cm^{-1} at 685 nm in MeCN). Computational results showed excellent agreement with the experimental data, indicating that the 600–800 nm absorption arises from charge transfer (CT) transitions between the donor (**TPA**) and the acceptor (**TOS**), while the 300–450 nm band corresponds to hybridized local excitation (π–π* transition) (Fig. S3 and S4). The photoluminescence (PL) spectrum of **TPA-TOS** in polar solvents closely resembled that of **TOS**, with a principal emission peak at 350–450 nm attributable to local excitation (LE) from the **TOS** moiety and a weak, broad peak around 590 nm (Fig. 3(b)). However, in nonpolar hexane, the emission intensity in the 350–400 nm region is markedly reduced, whereas a pronounced near-infrared (NIR) emission band centered at 703 nm emerges, accompanied by a shoulder at approximately 780 nm and an extended long-wavelength tail in the NIR region upon excitation at 300 nm (Fig. S5). Same NIR emission was observed under 650 nm excitation, confirming that this emission originates from the CT state, specifically TPA^{+}-TOS^{-},

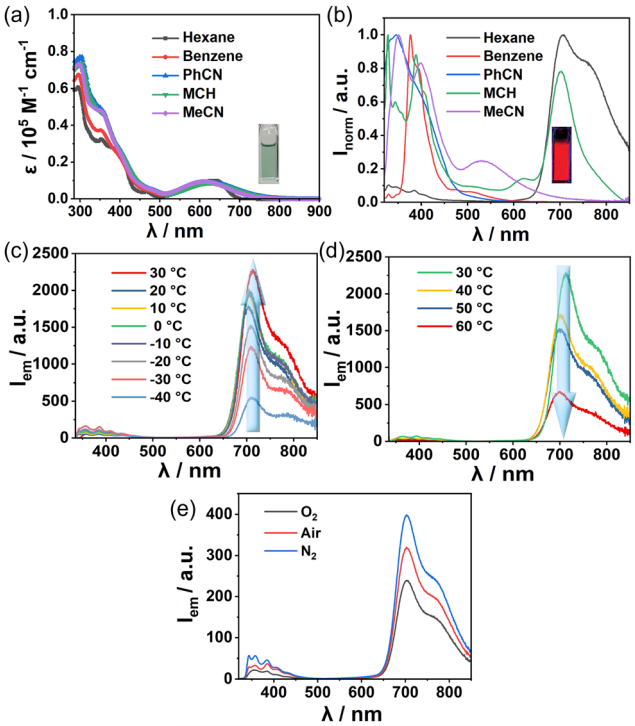

Fig. 3 Optical properties of **TPA-TOS**. (a) UV-vis-NIR absorption spectra of **TPA-TOS** in various solvents (c = 1.0 × 10^{-5} M). The inset photo was taken under general room light. (b) Photoluminescence spectra (λ_{ex} = 300 nm) of **TPA-TOS** in diluted solutions (c = 1.0 × 10^{-5} M). The inset photo was taken under a UV lamp (365 nm) in hexane at dark. Intensity is normalized at the wave length with the highest peak intensity. (c and d) Temperature-dependent photoluminescence spectra (λ_{ex} = 300 nm) of **TPA-TOS** (c = 1.0 × 10^{-5} M) in hexane (c) from −40 °C to 30 °C and (d) from 30 °C to 60 °C. (e) Effect of outer atmosphere on long wavelength emission of **TPA-TOS** at 300 K. PhCN: benzonitril, MCH: methylcyclohexane.

Table 1 Photophysical properties of **TPA-TOS**

Solvent	λ_{abs} [nm] (ε × 10^4 [M^{-1} cm^{-1}])	λ_{em} [nm][a] (Φ_{em})
Hexane	296 (6.1)	350 (0.01[b])
	643 (1.2)	703 (0.66[b], 0.34[c])
MeCN	300 (7.6)	355 (0.01[b])
	662 (1.2)	

[a] λ_{ex} = 320 nm at 300 K. [b] Under N_2 atmosphere. [c] Under O_2 atmosphere.

formed following photoexcitation (Fig. S6). The excitation spectrum demonstrated that **TPA-TOS** absorbs across nearly the entire visible range, enabling efficient NIR emission (Fig. S7). Relative to the weak emissive nature of **TOS** alone (Φ_{em}: 0.02 at 330 nm),[22] **TPA-TOS** exhibits a significantly enhanced fluorescence quantum yield of 0.66 at 703 nm in hexane under an N_2 atmosphere. Additionally, its NIR emission capability is robust in PMMA and Zeonex films, achieving Φ_{em} values of 0.32 and 0.74, respectively (Fig. S8). The possibility of aggregation-induced effects was denied by the concentration dependent PL spectra ranging from 10^{-6} to 10^{-3} M. As shown in the experimental spectra (Fig. S9(b)), the emission intensity

decreases with increasing concentration, indicating that the molecule exhibits general aggregation-induced quenching behaviour. No Tyndall scattering was neither observed in non-polar solvent systems.

To elucidate the origin of this strong NIR emission, various external factors influencing emission properties were investigated. Temperature-dependent PL measurements revealed a rise in emission intensity as the temperature increased from −40 °C to 30 °C, followed by a noticeable decline at temperatures exceeding 30 °C (Fig. 3(c) and (d)). This temperature-dependent behaviour is characteristic of systems where triplet states play a significant role in the emission process.[26–28] At relatively low temperatures, a moderate increase in temperature facilitates thermally activated processes, including enhanced reversible intersystem crossing, resulting in increased fluorescence intensity. Upon further increasing the temperature into this range, enhanced molecular vibrational and rotational motions promote non-radiative decay pathways, leading to increased energy dissipation and a subsequent decrease in fluorescence intensity. Atmospheric effects further verified the contribution of triplet states to the NIR emission of **TPA-TOS** (Fig. 3(e)). Phosphorescence at 749 nm was observed both in 2-methyltetrahydrofuran glass at 77 K and in Zeonex film, which overlapped with the lower-energy portion of the emission spectrum (Fig. S9 and S10). Collectively, these findings suggest that the observed NIR emission arises from both singlet (^{1}[**TPA$^+$-TOS$^-$**], ^{1}CT) and triplet (^{3}[**TPA$^+$-TOS$^-$**], ^{3}CT) components. Importantly, the energy gap between ^{1}CT and ^{3}CT (ΔE_{st}) was experimentally estimated to be <0.01 eV based on the fluorescence and phosphorescence emission spectra (Fig. S10a), implying efficient thermally activated delayed fluorescence (TADF) coupled with room-temperature phosphorescence (RTP), which is mainly reported in the solid state systems[29–31] and the solution-based ones are still rare.[32,33] This small ΔE_{ST} results from the effective spatial separation of the HOMO and LUMO (Fig. 2(b)) within the **TPA-TOS** system, underscoring the unique photophysical properties of TADF incorporating RTP in nonpolar environments such as hexane. As above discussion revealed the solvent dependency in the emission property of **TPA-TOS**, we measured the fluorescence spectra of **TPA-TOS** using a series of hexane–acetonitrile mixtures with varying polarity. It showed significant positive solvatofluorochromism as a function of the solvent permittivity (Fig. S11). A linear correlation between Stokes shift and Lippert–Mataga solvent polarizability revealed that the dipole moment at the excited state (μ_e) reached 54 Debye (33 Debye by DFT calculation at B3LYP/6-311G**), which is significantly larger than the ground-state dipole moment μ_g (3.41 Debye). This finding supported the formation of CT structure at the excited state with a large dipole moment. Moreover, the fluorescence intensity of **TPA-TOS** decreased with increasing solvent polarity, indicating that polar solvents accelerate non-radiative deactivation of the CT species involved in delayed fluorescence.

Transient absorption and time-resolved spectroscopy

To investigate the solvent-dependent photo-relaxation dynamics of **TPA-TOS**, femtosecond transient absorption (fsTA) measurements were performed in nonpolar hexane and polar acetonitrile (MeCN) (Fig. 4 and Table 2). Upon excitation at 343 nm, the fsTA maps during the initial 2 ps appeared similar in both solvents. Specifically, ultrafast spectral changes were observed, which are attributable to the localized excited (LE) state absorption originating from the **TPA** and **TOS** skeletons (Fig. 4(a) and (d)). This assignment aligns well with previously reported transient absorption (TA) spectra of **TOS**[22] and photo-excited **TPA**[34] (Fig. S12). Meanwhile, a broad absorption component around 700 nm, corresponding to charge transfer (CT) absorption associated with the formation of **TPA$^+$-TOS$^-$**, emerged in both solvents, indicating that fast CT processes occur even in nonpolar hexane. At longer timescales—after 5 ps in MeCN and 20 ps in hexane—a new absorption band emerged in the near-infrared (NIR) region beyond 900 nm, which

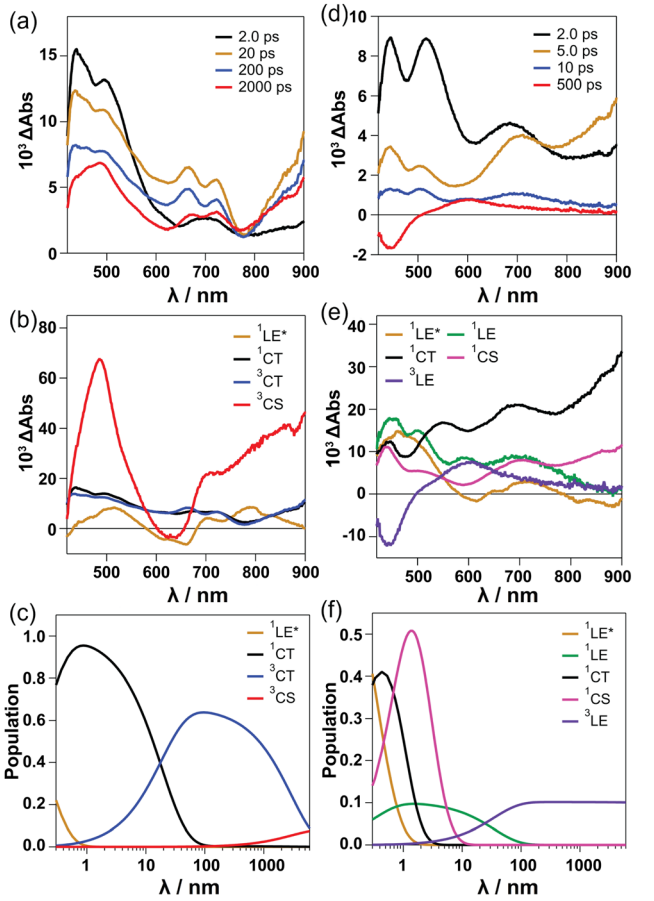

Fig. 4 Dynamic Optical properties of **TPA-TOS**. (a) and (d) fsTA spectra of **TPA-TOS**. (b and e) The species-associated spectra. (c) and (f) Time profiles of population change of each excited species. (a)–(c): obtained in hexane and (d)–(f): obtained in MeCN.

Table 2 Lifetime of each excited species

Solvent	^{1}LE*	^{1}LE	^{1}CT	^{3}CT	^{1}CS	^{3}CS	^{3}LE
Hexane	<410 fs	—	19 ps	2.9 ns	—	>6 ns	—
MeCN	<410 fs	550 fs	1.9 ps	—	34 ps	—	>6 ns

extended past 1000 nm as confirmed by picosecond transient absorption (psTA) measurements (Fig. S13). This long-wavelength absorption exceeding 1000 nm closely resembles the characteristic absorption of the **TOS** radical anion (**TOS**$^{\bullet-}$, 1040 nm).[19] Simultaneously, the characteristic dual absorption band of the **TPA** radical cation (**TPA**$^{\bullet+}$) appeared at 650–750 nm, corroborating previous reports on **TPA**$^{\bullet+}$ absorption spectra.[35] Taken together, these findings strongly support the generation of a charge-separated (CS) state, specifically **TPA**$^{\bullet+}$-**TOS**$^{\bullet-}$, in both hexane and MeCN. These solvent-independent CS state dynamics and their distinct spectral fingerprints provide direct insight into the photophysical behaviours underlying **TPA-TOS**, establishing its ability to undergo efficient charge separation and radical formation across a wide range of solvent polarities.

To further confirm the formation of the charge-separated (CS) state, electron spin resonance (ESR) measurements were conducted, which provided evidence for the generation of triplet radical species [^{3}(**TPA**$^{\bullet+}$-**TOS**$^{\bullet-}$)] (^{3}CS) (Fig. 5(a)). Upon photoirradiation of a hexane solution of **TPA-TOS** at 123 K with 365 nm UV light, an ESR signal was detected at g = 2.0049, along with a distinct zero-field splitting pattern—a hallmark of triplet state formation. This observation unequivocally confirmed the presence of the ^{3}CS species. The zero-field splitting parameter (D) was determined from the fine structure of the ESR spectrum to be 116 G (11.6 mT), which was much smaller than the reported D value of the ^{3}CT species of carbazole-based small D-A system, reflecting the longer spin–spin distance than the case of ^{3}CT state.[36] From this parameter, the distance (r) between the two unpaired electrons was calculated to be 6.2 Å,[37] consistent with previously reported spin–spin distances in similar triplet radical ion pairs. This calculated distance aligns well with the structural characteristics of the **TPA**$^+$-**TOS**$^-$ ^{3}CS species, further supporting its assignment as a triplet charge-separated state (Fig. 5(b)). These ESR findings provide direct evidence for the involvement of the triplet CS state in the photophysical processes of **TPA-TOS**.

A more detailed analysis revealed a striking difference in the fate of the photo-relaxation process depending on the solvent polarity. In nonpolar hexane, the charge-separated (CS) states exhibited lifetimes ranging from several thousand picoseconds to hundreds of microseconds (Fig. 4(a) and Fig. S13(c) and (d)), indicating that the relaxation pathway involved intersystem crossing (ISC) and reverse intersystem crossing (RISC) processes between the ^{1}CT and ^{3}CT states. In contrast, n polar MeCN, all excited states of **TPA-TOS** rapidly relaxed within 10 ps, ultimately producing a weak broad absorption band around 600 nm after 500 ps, likely attributable to the previously reported triplet state of **TOS** (Fig. S12(b)).[22] This rapid decay process in MeCN, lacking ^{1}CT emission, suggests a competition between two relaxation pathways: one leading to the ^{3}LE state *via* the ^{1}LE state, and the other proceeding to the ^{1}CS state through fast electron transfer from the **TPA** to the **TOS** moiety of the ^{1}CT species. Based on these assumptions, the best-fitting results revealed the involvement of ^{1}LE, ^{3}LE, ^{1}CT, and ^{1}CS states in the MeCN solution, while additional states—^{3}CT and ^{3}CS—were found to contribute to the hexane solution (Fig. 4(b), (c), (e) and (f)). The proposed emission mechanisms, depending on the solvent system, are summarized in Fig. 6. The results further clarified key rate dynamics. In hexane, the ISC rate from the ^{1}CT to ^{3}CT state (k_{3CT}: 3.53 × 10^{10} s^{-1}) was higher than the fluorescence rate from the ^{1}CT state ($k_{LUM}{}^1$: 1.81 × 10^{10} s^{-1}),

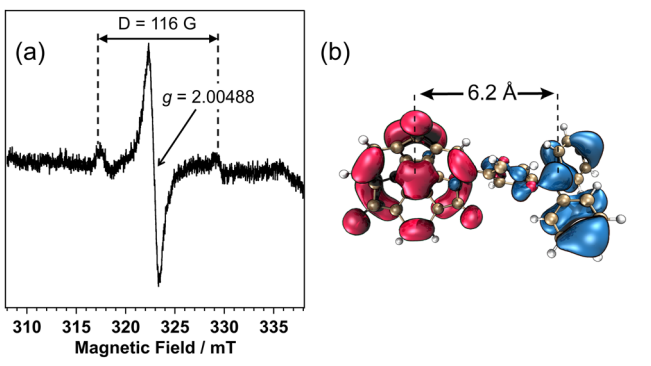

Fig. 5 Radical ion pair of **TPA-TOS**. (a) ESR spectrum of **TPA-TOS** (5 × 10^{-4} M) in deaerated hexane after 365 nm photoirradiation at 123 K. (b) Scheme of radical ion pair distance. Spin density plot of was calculated as [^{3}(**TPA**$^{\bullet+}$-**TOS**$^{\bullet-}$)] at UB3LYP/6-311+(d,p).

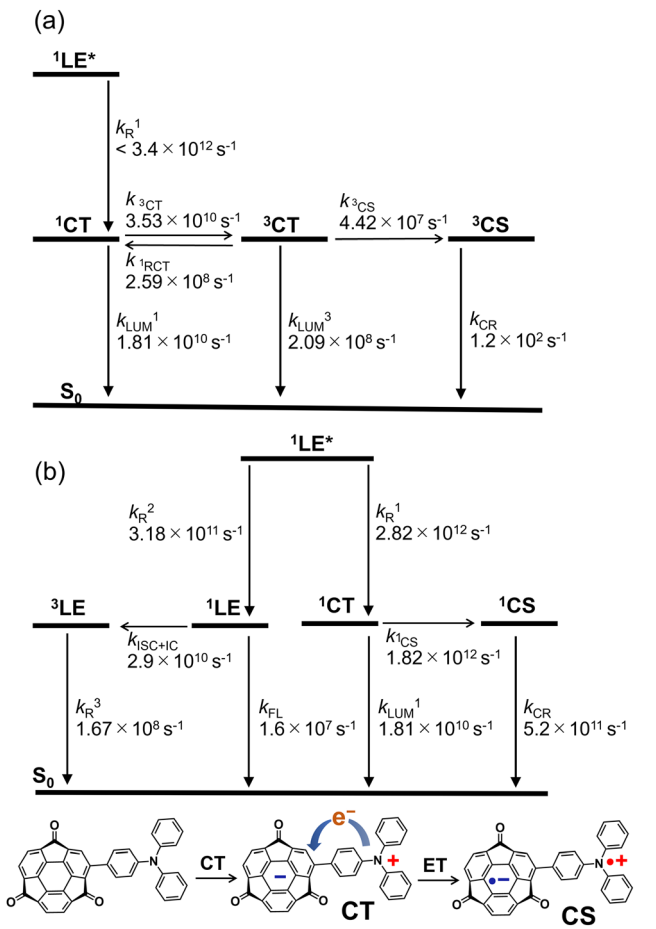

Fig. 6 Energy-level diagram of **TPA-TOS**. (a) Schematic illustration of the excited-state energy relationships of **TPA-TOS** in hexane. (b) Schematic illustration of the excited-state energy relationships of **TPA-TOS** in MeCN.

explaining the negligible emission intensity from the ^{1}LE state. Another noteworthy observation is that the RISC rate from the ^{3}CT to ^{1}CT state (k_{1RCT}: 2.59 × 10^8 s^{-1}) was nearly identical to the phosphorescence rate ($k_{LUM}{}^3$: 2.09 × 10^8 s^{-1}), facilitating efficient thermally activated delayed fluorescence (TADF) alongside phosphorescence emission to give high Φ_{em} reaching more than 0.60. Such coexistence of TADF and room-temperature phosphorescence (RTP) is relatively rare, particularly in solution systems.[38] Considering the case in MCH and benzene, probably the population of TADF and RTP path is likely controlled by the solvent systems with relatively low polarity, which will be our future work (Fig. 3(b)). The relaxation pathway from the ^{3}CT state to the ^{3}CS state was slower by an order of magnitude compared to the RISC process, resulting in only a small fraction of the excitons reaching the CS state as their final destination. These CS-state excitons transitioned slowly to the ground state *via* charge recombination (k_{CR}: 1.2 × 10^2 s^{-1}). Conversely in MeCN, two competitive fast relaxation pathways were observed: one leading to the ^{1}CT state ($k_R{}^1$: 2.82 × 10^{12} s^{-1}) and the other to the ^{1}LE state ($k_R{}^2$: 3.18 × 10^{11} s^{-1}). The faster charge transfer process quickly transitioned to the ^{1}CS state (k_{1CS}: 1.82 × 10^{12} s^{-1}), followed by charge recombination (k_{CR}: 5.2 × 10^{11} s^{-1}) due to a significant stabilization of CT and CS states in polar solvent. On the other hand, the slower relaxation path to the ^{1}LE state eventually reached the ^{3}LE state *via* ISC (k_{ISC+IC}: 2.9 × 10^{10} s^{-1}), exhibiting negligible fluorescence emission (k_{FL}: 1.6 × 10^7 s^{-1}).

Plausible discussion about the effect of the curved-π structure

Considering that previously reported materials exhibiting long-CS lifetimes often feature a C_{60} skeleton, and that the curved-π systems typically display large spin–orbital coupling which accelerates ISC, it is reasonable to have interest in the contribution of the sumanene skeleton for the relevant phenomena. To tackle this mystery, we conducted density functional theory (DFT) calculation. While several benchmarking studies have suggested recommended computational methods for the excited-state properties of intramolecular CT systems, it was found that the methodological dependence of **TPA-TOS** is rather complex due to its extended π-conjugation system. Indeed, as already applied in the evaluation of UV-vis absorption measurement results, TD-RB3LYP/6-311G(d,p) level of theory well reproduced the experimental CT band around 600–800 nm, although the excitation energy appears to be underestimated to some extent. This method also predicted the dihedral angle θ-dependent S_1–T_1 gap (ΔE_{ST}) and $\Delta E_{ST} \sim 0$ around $\theta = 90^\circ$. The S_1 potential energy curve was nearly flat in the range of $30^\circ \leq \theta \leq 120^\circ$, and the geometry optimization for the S_1 state converged to a structure with $\theta \sim 90^\circ$ (Fig. 7). This result supports experimental observation. However, further theoretical investigation revealed significant dependence on the function used, which prevents us from drawing more detailed conclusions how bowl shape of sumanene contributed the effective ISC and the high stability of CS state with μs-ordered lifetime at this stage (see SI). Nevertheless, the effect of curved-π structure of sumanene cannot be overlooked, as it at least contributed to; (1) high solubility of **TPA-TOS** even in non-polar hexane; (2) possessed a large |SOC| to accelerate ISC between ^{1}CT and ^{3}CT, supporting effective TADF and RTP to give high quantum yield, as well as long life time of the CS state. Although additional theoretical refinement is required to fully understand the impact of the sumanene skeleton and its bowl-shaped geometry, the experimental and theoretical findings suggest that this unique curved-π architecture plays a pivotal role in enhancing the photophysical performance of **TPA-TOS**. Indeed, such novel effect of the curved structure has also been confirmed in pristine **TOS**[22] and recently reported *N*-pyrrolic polycyclic aromatic hydrocarbons.[39] In the present case, the curved-π skeleton supports not only efficient ISC and TADF/RTP processes with high quantum yield, but also the observed long-lived CS state, which could have significant implications for applications in advanced photonic and optoelectronic devices.

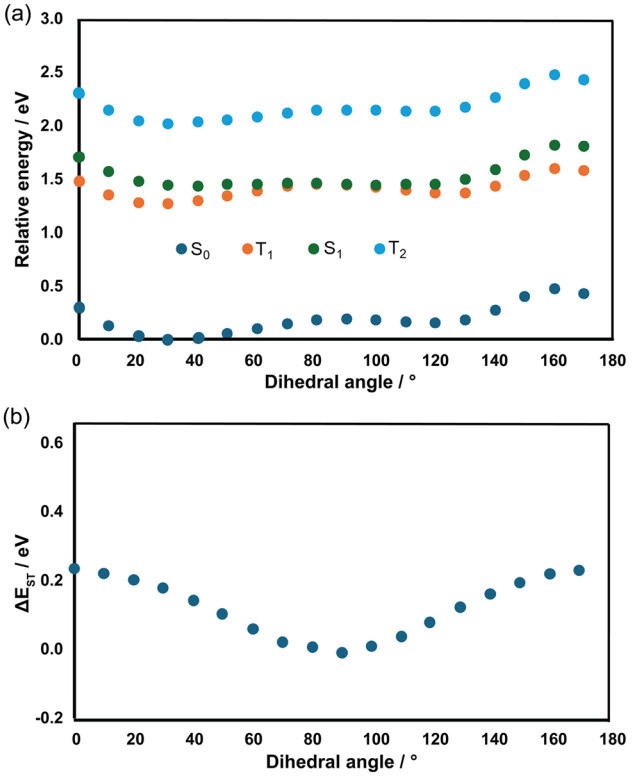

Fig. 7 Preliminary energy evaluation depending on the dihedral angle between **TPA** and **TOS** moieties. (a) The dihedral angle-dependent relative energy of S_0, S_1, T_1, T_2 states. (b) The S_1–T_1 gap (ΔE_{ST}) of **TPA-TOS** was calculated at TD-RB3LYP/6-311G(d,p) level of theory.

Conclusions

In this study, we have developed a novel donor–acceptor (D–A) near-infrared (NIR) dye, **TPA-TOS**, featuring a rigid bowl-shaped acceptor, **TOS**, and a strong donor, **TPA**, without relying on long-range conjugation or complex multi-donor/acceptor systems. This unique molecular design successfully establishes an effective TADF and RTP system, enabling high-efficiency NIR

emission with an impressive quantum yield. Remarkably, the exciton in nonpolar hexane proceeds through efficient charge separation, reaching a long-lived CS state despite the short D–A distance. Conversely, in polar MeCN, the CS state becomes short-lived due to faster relaxation dynamics. Although further theoretical studies are required for a deeper understanding, the curved **TOS** framework clearly contributes to the observed photophysics, providing a high solubility in non-polar hexane, large |SOC| to accelerate ISC between ^{1}CT and ^{3}CT states, giving rise to TADF and RTP. This unique design and the remarkable photophysical characteristics of **TPA-TOS** open new avenues for the development of efficient NIR dyes with innovative molecular architectures. By overcoming conventional limitations of D–A systems, this work provides a promising platform for future advancements in optoelectronic applications and deepens understanding of charge separation dynamics in tailored curved-π systems.

Author contributions

Han Junyi, Yumi Yakiyama and Hidehiro Sakurai: conceptualization. Han Junyi, Yumi Yakiyama and Hayato Sakai: validation. Han Junyi, Yumi Yakiyama, Hayato Sakai, Youhei Takeda, Ryohei Kishi and Kei Ohkubo: investigation. Han Junyi and Yumi Yakiyama: writing – original draft. Han Junyi, Yumi Yakiyama, Hayato Sakai, Taku Hasobe, Youhei Takeda, Ryohei Kishi, Kei Ohkubo and Hidehiro Sakurai: writing – review & editing. Yumi Yakiyama, Ryohei Kishi, Kei Ohkubo and Hidehiro Sakurai: funding acquisition. Yumi Yakiyama, Hayato Sakai and Hidehiro Sakurai: supervision.

Conflicts of interest

There are no conflicts to declare.

Data availability

The authors confirm that the data supporting the findings of this study are available within the article and its SI. Experimental raw data were generated at The university of Osaka and Keio University. Derived data supporting the findings of this study are available from the corresponding author Y. Y. on request.

Supplementary information (SI) including synthetic details, NMR, MS, PL, TA spectra and DFT calculation detail is available. See DOI: **https://doi.org/10.1039/d5qm00818b**.

Acknowledgements

This work was supported by Grant-in-Aid for Scientific Research on Innovative Areas ''π Space Figuration'' (No. JP26102002), Grant-in-Aid for Transformative Research Areas ''Science of 2.5 Dimensional Materials'' (No. JP21H05233), JSPS KAKENHI (No. JP19H00912, JP22H04974, JP22H02050, JP23K04708, JP24K01473, JP24H00460, JP24K21770), and Dynamic Alliance for Open Innovation Bridging Human, Environment and Materials (No. 20224023, 20234025 and 20254019). The theoretical calculations were performed at the Research Center for Computational Science, Okazaki, Japan (22-IMS-C068, 25-IMS-C004, and 25-IMS-C060). Y. Y. is grateful for support from the Masuyakinen basic research foundation. Y. Y. and R. K. are grateful for support from the program ''Collaborative Research Grants for Young Researchers'', ICS-OTRI, The University of Osaka. J. H. thanks the Otsuka Toshimi Scholarship Foundation for kindly providing scholarships (19-S5 and 20-S4). The authors appreciate Prof. Manabu Abe (Hiroshima Univ.) for the fruitful discussion about the relaxation path of **TPA-TOS**.

Notes and references

1 A. Khasbaatar, Z. Xu, J.-H. Lee, G. Campillo-Alvarado, C. Hwang, B. N. Onusaitis and Y. Diao, From solution to thin film: molecular assembly of π-conjugated systems and impact on (opto) electronic properties, *Chem. Rev.*, 2023, **123**, 8395–8487.

2 M. Zhao, M. Li, W. Li, S. Du, Z. Chen, M. Luo, Y. Qiu, X. Lu, S. Yang and Z. Wang, Highly Efficient Near-Infrared Thermally Activated Delayed Fluorescent Emitters in Non-Doped Electroluminescent Devices, *Angew. Chem., Int. Ed.*, 2022, **61**, e202210687.

3 X. Liu, S. Dai, Y. Jin, J. Zhang, Z. Guo, T. Sun, L. Li, P. Guo, H. Gao, H. Liang, S. Zhang, L. Xiong, Y. Zhou and J. Huang, Near-infrared organic photoelectrochemical synaptic transistors by wafer-scale photolithography for neuromorphic visual system, *Nat. Commun.*, 2025, **17**, 197.

4 L. Zheng, W. Na, F. Gao and C. Ou, Boosting fluorescence efficiency of NIR-II dyes for multifunctional fluorescence imaging via hydrogen bonding, *Mater. Chem. Front.*, 2025, **9**, 1547–1558.

5 R. Weinstain, T. Slanina, D. Kand and P. Klan, Visible-to-NIR-light activated release: from small molecules to nanomaterials, *Chem. Rev.*, 2020, **120**, 13135–13272.

6 L. Wang, W. Du, Z. Hu, K. Uvdal, L. Li and W. Huang, Hybrid rhodamine fluorophores in the visible/NIR region for biological imaging, *Angew. Chem., Int. Ed.*, 2019, **58**, 14026–14043.

7 P. Brogdon, H. Cheema and J. H. Delcamp, Near-infrared-absorbing metal-free organic, porphyrin, and phthalocyanine sensitizers for panchromatic dye-sensitized solar cells, *ChemSusChem*, 2018, **11**, 86–103.

8 P. L. dos Santos, P. Stachelek, Y. Takeda and P. Pander, Recent advances in highly-efficient near infrared OLED emitters, *Mater. Chem. Front.*, 2024, **8**, 1731–1766.

9 P. M. Beaujuge, W. Pisula, H. N. Tsao, S. Ellinger, K. Müllen and J. R. Reynolds, Tailoring structure– property relationships in dithienosilole– benzothiadiazole donor– acceptor copolymers, *J. Am. Chem. Soc.*, 2009, **131**, 7514–7515.

10 J. D. Yuen, R. Kumar, D. Zakhidov, J. Seifter, B. Lim, A. J. Heeger and F. Wudl, Ambipolarity in Benzobisthiadiazole-

Based Donor–Acceptor Conjugated Polymers, *Adv. Mater.*, 2011, **23**, 3780.

11 T. Steckler, M. Lee, Z. Chen, O. Fenwick, M. R. Andersson, F. Cacialli and H. Sirringhaus, Multifunctional materials for OFETs, LEFETs and NIR PLEDs, *J. Mater. Chem. C*, 2014, **2**, 5133–5141.

12 P. Murto, A. Minotto, A. Zampetti, X. Xu, M. R. Andersson, F. Cacialli and E. Wang, Triazolobenzothiadiazole-Based Copolymers for Polymer Light-Emitting Diodes: Pure Near-Infrared Emission via Optimized Energy and Charge Transfer, *Adv. Opt. Mater.*, 2016, **4**, 2068–2076.

13 K. Narayanaswamy, A. Venkateswararao, V. Gupta, S. Chand and S. P. Singh, NIR absorbing D–π–A–π–D structured diketopyrrolopyrrole–dithiafulvalene based small molecule for solution processed organic solar cells, *Chem. Commun.*, 2016, **52**, 210–213.

14 Y. Zhang, S. K. Hau, H.-L. Yip, Y. Sun, O. Acton and A. K.-Y. Jen, Efficient polymer solar cells based on the copolymers of benzodithiophene and thienopyrroledione, *Chem. Mater.*, 2010, **22**, 2696–2698.

15 J. T. Buck, A. M. Boudreau, A. DeCarmine, R. W. Wilson, J. Hampsey and T. Mani, Spin-allowed transitions control the formation of triplet excited states in orthogonal donor-acceptor dyads, *Chem*, 2019, **5**, 138–155.

16 R. Kumar, H. Aggarwal and A. Srivastava, Of twists and curves: Electronics, photophysics, and upcoming applications of non-planar conjugated organic molecules, *Chem. – Eur. J.*, 2020, **26**, 10653–10675.

17 Q. Xu, Y. Wang, Y. Guan, C. Ma, G. Yi, X. Du, H. Bin, W. Shen, C. Y. Wang and Y. Wu, Hybrid Planar–Twisted Chair-Shaped Indoline Donor Enabling Bright Molecular and Aggregated State Near-Infrared Emission, *Angew. Chem., Int. Ed.*, 2025, e22144.

18 J. Sun, Y. Sun, C. Yan, D. Lin, Z. Xie, S. Zhou, C. Yuan, H.-L. Zhang and X. Shao, Remarkable nonlinear optical response of pyrazine-fused trichalcogenasumanenes and their application for optical power limiting, *J. Mater. Chem. C*, 2018, **6**, 13114–13119.

19 S. Higashibayashi, B. B. Shrestha, Y. Morita, M. Ehara, K. Ohkubo, S. Fukuzumi and H. Sakurai, Sumanenetrione anions generated by electrochemical and chemical reduction, *Chem. Lett.*, 2014, **43**, 1297–1299.

20 T. Amaya, M. Hifumi, M. Okada, Y. Shimizu, T. Moriuchi, K. Segawa, Y. Ando and T. Hirao, Synthesis of oxosumanenes through benzylic oxidation, *J. Org. Chem.*, 2011, **76**, 8049–8052.

21 J. Han, Y. Uetake, Y. Yakiyama and H. Sakurai, Derivatization of sumanenetrione through Lewis acid-mediated Suzuki–Miyaura coupling and an unprecedented ring opening, *Chem. Commun.*, 2023, **59**, 4632–4635.

22 K. Kanahara, M. M. R. Badal, S. Hatano, M. Abe, S. Higashibayashi, N. Takashina and H. Sakurai, Intra-and intermolecular reactivity of triplet sumanenetrione, *Bull. Chem. Soc. Jpn.*, 2015, **88**, 1612–1617.

23 J. Sworakowski, How accurate are energies of HOMO and LUMO levels in small-molecule organic semiconductors determined from cyclic voltammetry or optical spectroscopy?, *Synth. Met.*, 2018, **235**, 125–130.

24 E. T. Seo, R. F. Nelson, J. M. Fritsch, L. S. Marcoux, D. W. Leedy and R. N. Adams, Anodic oxidation pathways of aromatic amines. Electrochemical and electron paramagnetic resonance studies, *J. Am. Chem. Soc.*, 1966, **88**, 3498–3503.

25 M. Soltani, R. Minakar, H. R. Memarian and H. Sabzyan, Cyclic voltammetric study of 3, 5-diaryl-1-phenyl-2-pyrazolines, *J. Phys. Chem. A*, 2019, **123**, 2820–2830.

26 N. Aizawa, A. Matsumoto and T. Yasuda, Thermal equilibration between singlet and triplet excited states in organic fluorophore for submicrosecond delayed fluorescence, *Sci. Adv.*, 2021, **7**, eabe5769.

27 T. Kobayashi, A. Niwa, K. Takaki, S. Haseyama, T. Nagase, K. Goushi, C. Adachi and H. Naito, Contributions of a higher triplet excited state to the emission properties of a thermally activated delayed-fluorescence emitter, *Phys. Rev. Appl.*, 2017, **7**, 034002.

28 J. M. Dos Santos, D. Hall, B. Basumatary, M. Bryden, D. Chen, P. Choudhary, T. Comerford, E. Crovini, A. Danos and J. De, The golden age of thermally activated delayed fluorescence materials: design and exploitation, *Chem. Rev.*, 2024, **124**, 13736–14110.

29 Y. Xiong, J. Gong, J. Liu, D. Wang, H. Wu, Z. Zhao, M. Fang, Z. Li, D. Wang and B. Z. Tang, Achieving diversified emissive behaviors of AIE, TADF, RTP, dual-RTP and mechanoluminescence from simple organic molecules by positional isomerism, *J. Mater. Chem. C*, 2022, **10**, 10009–10016.

30 L. Zhan, Z. Chen, S. Gong, Y. Xiang, F. Ni, X. Zeng, G. Xie and C. Yang, A simple organic molecule realizing simultaneous TADF, RTP, AIE, and mechanoluminescence: understanding the mechanism behind the multifunctional emitter, *Angew. Chem.*, 2019, **131**, 17815–17819.

31 L. Huang, L. Liu, X. Li, H. Hu, M. Chen, Q. Yang, Z. Ma and X. Jia, Crystal-state photochromism and dual-mode mechanochromism of an organic molecule with fluorescence, room-temperature phosphorescence, and delayed fluorescence, *Angew. Chem., Int. Ed.*, 2019, **58**, 16445–16450.

32 S. Dey, M. Hasan, A. Shukla, N. Acharya, M. Upadhyay, S.-C. Lo, E. B. Namdas and D. Ray, Thermally activated delayed fluorescence and room-temperature phosphorescence in asymmetric phenoxazine-quinoline (D2–A) conjugates and dual electroluminescence, *J. Phys. Chem. C*, 2022, **126**, 5649–5657.

33 I. Bhattacharjee, N. Acharya, H. Bhatia and D. Ray, Dual emission through thermally activated delayed fluorescence and room-temperature phosphorescence, and their thermal enhancement via solid-state structural change in a carbazole-quinoline conjugate, *J. Phys. Chem. Lett.*, 2018, **9**, 2733–2738.

34 F. Chen, Q. Yu, Y. Guo and M. Fan, Photophysical Studies on Organic-Compounds-Time-Resolved Transient Absorption-Spectra Studies on Triphenylamine in Various Solvents, *Sci. China: Chem.*, 1991, **34**, 135–140.

35 O. Yurchenko, D. Freytag, L. zur Borg, R. Zentel, J. R. Heinze and S. Ludwigs, Electrochemically induced reversible and irreversible coupling of triarylamines, *J. Phys. Chem. B*, 2012, **116**, 30–39.
36 B. H. Drummond, N. Aizawa, Y. Zhang, W. K. Myers, Y. Xiong, M. W. Cooper, S. Barlow, Q. Gu, L. R. Weiss and A. J. Gillett, Electron spin resonance resolves intermediate triplet states in delayed fluorescence, *Nat. Commun.*, 2021, **12**, 4532.
37 M. Abe, Diradicals, *Chem. Rev.*, 2013, **113**, 7011–7088.
38 P. Xu, R. Hojo and Z. M. Hudson, Thermally Activated Delayed Fluorescence and Room-Temperature Phosphorescence in Materials with Imidazo-pyrazine-5, 6-dicarbonitrile Acceptors, *Chem. – Eur. J.*, 2023, **29**, e202203585.
39 J. Wagner, P. Zimmermann Crocomo, M. A. Kochman, A. Kubas, P. Data and M. Lindner, Modular Nitrogen-Doped Concave Polycyclic Aromatic Hydrocarbons for High-Performance Organic Light-Emitting Diodes with Tunable Emission Mechanisms, *Angew. Chem.*, 2022, **134**, e202202232.

